Entropy-driven crystal formation on highly strained substrates

John R. Savage[a], Stefan F. Hopp[b], Rajesh Ganapathy[a], Sharon J. Gerbode[a], Andreas Heuer[b], and Itai Cohen[a,1]

[a]Department of Physics, Cornell University, Ithaca, NY 14853; and [b]Institut für Physikalische Chemie, Universität Münster, DE-48149 Münster, Germany

Edited by David A. Weitz, Harvard University, Cambridge, MA, and approved April 15, 2013 (received for review December 10, 2012)

In heteroepitaxy, lattice mismatch between the deposited material and the underlying surface strongly affects nucleation and growth processes. The effect of mismatch is well studied in atoms with growth kinetics typically dominated by bond formation with interaction lengths on the order of one lattice spacing. In contrast, less is understood about how mismatch affects crystallization of larger particles, such as globular proteins and nanoparticles, where interparticle interaction energies are often comparable to thermal fluctuations and are short ranged, extending only a fraction of the particle size. Here, using colloidal experiments and simulations, we find particles with short-range attractive interactions form crystals on isotropically strained lattices with spacings significantly larger than the interaction length scale. By measuring the free-energy cost of dimer formation on monolayers of increasing uniaxial strain, we show the underlying mismatched substrate mediates an entropy-driven attractive interaction extending well beyond the interaction length scale. Remarkably, because this interaction arises from thermal fluctuations, lowering temperature causes such substrate-mediated attractive crystals to dissolve. Such counterintuitive results underscore the crucial role of entropy in heteroepitaxy in this technologically important regime. Ultimately, this entropic component of lattice mismatched crystal growth could be used to develop unique methods for heterogeneous nucleation and growth of single crystals for applications ranging from protein crystallization to controlling the assembly of nanoparticles into ordered, functional superstructures. In particular, the construction of substrates with spatially modulated strain profiles would exploit this effect to direct self-assembly, whereby nucleation sites and resulting crystal morphology can be controlled directly through modifications of the substrate.

thermodynamics | colloids | tunable depletion interaction

Crystal growth typically initiates at surfaces where the barrier for nucleation is significantly lower than in bulk (1–5). If the surface is regular, lattice mismatch between the crystallizing material and the underlying substrate can strongly affect the resulting crystal morphology (6–10). In many systems of interest, including nanoparticles and globular proteins, the interparticle interactions extend only a small percent of the particle diameter (11–15). Consequently, even a small lattice mismatch should strongly frustrate particle configurations due to the competition between in-plane and substrate bonds. These effects are even more dominant at large mismatch, where particles at adjacent lattice sites are separated by distances greater than the interaction length. Overcoming these effects, however, is technologically important for many applications, including protein crystallization and assembly of photonic as well as photovoltaic devices (10, 16). Experimentally, these effects are difficult to study in situ at the nanometer scale due to rapid motions of particles and resolution limitations. Using micrometer-size colloidal particles has proved invaluable to investigate such phenomena because individual particle motions can be directly visualized (12, 17–25). Here we use colloids to study the competition between entropy and energy during crystallization on substrates of increasing lattice mismatch. A major experimental hurdle is the ability to change the interactions between particles in situ. We overcome this hurdle by using a system where we can change the strength of the attractive interactions. By increasing the strength of the interaction, a dilute suspension of colloidal particles can form locally dense ordered structures known as colloidal crystals. In addition, using Monte Carlo simulations we show the relative contributions of energy and entropy to the free energy depend sensitively on temperature, leading to unexpected phase behavior.

Results

Our system consists of 1.30-μm diameter charge stabilized polystyrene spheres in aqueous solution. The solution contains the nonionic surfactant, hexaethylene glycol monodocecyl ether ($C_{12}E_6$), which forms micelles in water. The micelles induce an attractive depletion interaction between polystyrene spheres for surface-to-surface distances of approximately one micelle diameter or less. The depth of the interaction potential is proportional to the entropy gained due to the volume liberated to the micelles when the excluded volume around the two particles overlaps with strength of a few k_BT, where k_B is Boltzmann's constant and T is temperature. This interaction is strongly dependent on both the concentration and the diameter of the micelles. By using the surfactant $C_{12}E_6$, whose micelle concentration and diameter both increase with increasing temperature, small temperature changes allow the particles to overcome thermal fluctuations and form colloidal crystals (24, 25). Importantly, gravity is weak compared with thermal fluctuations, and a single layer of polystyrene spheres (density 1.055 g/cm^3) will not remain on the surface of the underlying layer in aqueous solution without the implementation of the depletion potential.

To study the role of strain in heterogeneous crystallization, a single layer of particles is first self-assembled in the holes of a lithographically patterned template (19, 23). The excluded volume liberated when particles are positioned in the patterned holes is larger than that liberated when particles interact with each other or a flat surface. Accordingly, the interaction strength is tuned so only particle–hole interactions overcome thermal fluctuations. Thus, a single crystalline layer possessing the symmetry and lattice spacing of the patterned template is formed. The remaining particles (area fraction ~0.15) diffuse on top of this crystalline layer, forming a weakly interacting 2D gas. A second temperature quench increases the strength of the interaction, causing the particles in this second layer to form crystals. In the experiments, the final temperature is kept constant at approximately 37 °C with micelles of diameter approximately 40 nm, as measured with dynamic light scattering.

In the experiments, we use bright-field microscopy to monitor how interparticle spacing in growing crystals varies with the

Author contributions: J.R.S., S.F.H., R.G., S.J.G., A.H., and I.C. designed research; J.R.S., S.F.H., and A.H. performed research; S.J.G. contributed new reagents/analytic tools; J.R.S., S.F.H., S.J.G., A.H., and I.C. analyzed data; and J.R.S., S.F.H., S.J.G., A.H., and I.C. wrote the paper.

The authors declare no conflict of interest.

This article is a PNAS Direct Submission.

[1]To whom correspondence should be addressed. E-mail: itai.cohen@cornell.edu.

This article contains supporting information online at www.pnas.org/lookup/suppl/doi:10.1073/pnas.1221529110/-/DCSupplemental.

lattice constant of the underlying substrate. Single-layer crystals were first assembled on a featureless microscope coverslip. The equilibrium lattice constant was obtained by measuring the nearest-neighbor separation probability distribution, $P(r)$. We find $P(r)$ is symmetric, peaks at $l_0 \sim 1.35$ μm, and decays to zero within 25 nm. This equilibrium lattice constant l_0 was compared with $P(r)$ for all particles on substrates with square and rectangular lattice symmetries having lattice constants ranging between 1.350 and 1.500 μm. Images and $P(r)$ measurements on substrates with square symmetry and three different lattice parameters are shown in Fig. 1. To quantify the role of strain in determining the resulting lattice constant of the crystals, we define the substrate and particle strains $\gamma_s = (l_s - l_0)/l_0$ and $\gamma_p = (l_p - l_0)/l_0$, respectively, where l_s is the underlying substrate lattice constant, and l_p corresponds to the peak(s) of the nearest-neighbor distribution $P(r)$. For a lattice constant of 1.375 μm ($\gamma_s = 0.019$)—a separation equal to the maximum range of the interaction—we observe highly ordered crystals with a wide distribution in size. The peak of $P(r)$ is commensurate with the lattice constant of the underlying substrate (Fig. 1*A*). Particle fluctuations are symmetric about the peak of $P(r)$ and decay to zero within 30 nm. At these strains, crystal size appears to be limited only by the number of available particles. Remarkably, as the lattice constant of the underlying substrate is increased to 1.425 μm ($\gamma_s = 0.074$)—a separation much greater than the interaction length scale—we still observe crystal formation. Energetically, bond counting suggests the most favorable configuration consists of particles residing at random lattice sites of the underlying substrate. Instead, we find $P(r)$ is bimodal characterized by two γ_p values, with one peak at 1.375 μm and the other less prominent peak near the underlying lattice constant of 1.425 μm (Fig. 1*B*). Correspondingly, the observed crystals are considerably smaller, with a maximum observed size of approximately 20 particles, and exhibit larger fluctuations in particle positions. As the lattice constant of the underlying substrate is increased further to 1.500 μm ($\gamma_s = 0.111$), the lower peak value l_p decreases significantly to ~1.32 μm, indicating the onset of a structural square-to-hexagonal transition in which many particles dewet from the substrate and form clusters having hexagonal symmetry (Fig. 1*C*). The apparent decrease of l_p from the equilibrium 1.35 μm is due to image processing, which accounts only for particles' lateral positions. Once dewetting occurs, particle centers can appear closer than particle diameters due to variation in particle heights. Fig. 2 shows the observed trends for particle strain γ_p as a function of increasing substrate strain γ_s for all our data on square substrates.

To uncover the mechanism of crystal formation on highly strained substrates, we fabricated templates with uniaxial strain to compare growth along the strained and unstrained directions. Fig. 3*A* shows crystals formed on a uniaxially strained substrate with a lattice constant of 1.500 μm along the strained direction. At this uniaxial strain, crystals tend to be anisotropic, with most bonds forming along the unstrained direction. To measure the free-energy cost of dimer formation along the strained direction relative to the unstrained direction, $\Delta F_{s/us}$, we measure the ratio of the number of dimers aligned along the strained and unstrained directions, $n_s/n_{us} = \exp(-\Delta F_{s/us}/k_BT)$. Here, we define a dimer as two isolated particles whose interparticle distance is less than two lattice spacings apart, thus having no other in-plane bonds. To determine how $\Delta F_{s/us}/k_BT = -\ln(n_s/n_{us})$ varies with increasing uniaxial strain, we plot $\Delta F_{s/us}/k_BT$ vs. γ_s in Fig. 3*B*. With increasing uniaxial strain, $\Delta F_{s/us}/k_BT$ remains small and constant at small strains and then increases monotonically and finally saturates near 1.5 at $\gamma_s \sim 0.074$. Notably, saturation coincides with the strain at which dewetting occurs. If bond formation were caused only by the two-particle interaction, then $\Delta F_{s/us}/k_BT$ would saturate at $\gamma_s \sim 0.02$, corresponding to the maximal range of the depletion potential. However, our results clearly indicate dimer formation along the strained direction at length scales much greater than the depletion interaction, suggesting the substrate plays a significant role in mediating interparticle interactions.

To identify how entropic and energetic contributions to particle interactions vary with substrate strain, we performed Monte Carlo simulations of particle pairs on substrates of both isotropic and uniaxial strains. The depletion interaction is modeled by the temperature-independent Morse potential $U(r) = E_0[1 - \exp(-a(r - l_0))]^2 - E_0$, where E_0 is the depth of the potential, $l_0 = 1.0$, and a is inversely proportional to the width of the potential. This interaction is applied to all particles, including both in-plane interactions and particle interactions with the underlying substrate, to faithfully reproduce the experiments. As seen in the experiments, gravity is weak compared with the interaction potential—

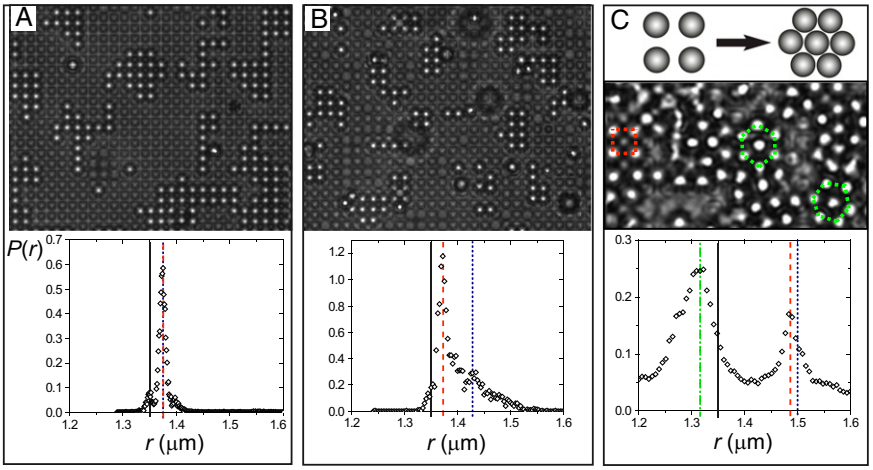

Fig. 1. Crystallization on isotropically strained square substrates. (*A*) Image and nearest-neighbor distribution $P(r)$ for crystals formed on a substrate with underlying lattice constant 1.375 μm (blue dotted line). The peak of $P(r)$ (red dashed line) is commensurate with the underlying substrate. (*B*) Image and $P(r)$ for crystals formed on a substrate with lattice constant 1.425 μm. $P(r)$ begins to exhibit a bimodal distribution. (*C*) Cartoon and image showing a square-to-hexagonal transition along with $P(r)$ for a substrate with lattice constant 1.500 μm (blue dotted line). The two peaks in $P(r)$ correspond to particles with square (red dashed line) and hexagonal (green dashed-dotted line) symmetries, respectively. The black line represents the equilibrium lattice constant for crystals formed on a flat surface.

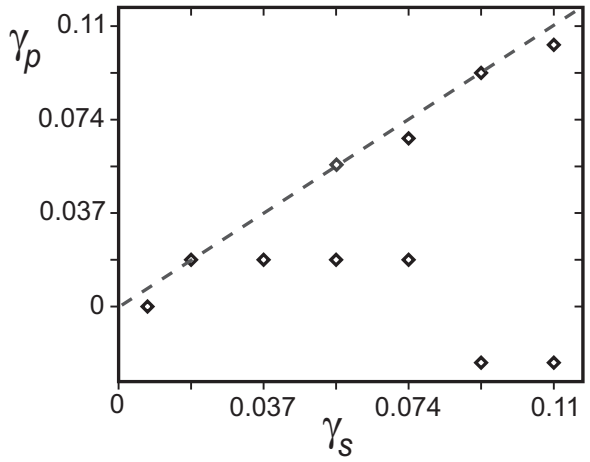

Fig. 2. Particle strain determined by the peak(s) of $P(r)$ for increasing substrate strain. For small substrate strains, γ_s and particle strain γ_p are nearly equal. At intermediate substrate strains, the nearest-neighbor distance distribution $P(r)$ is bimodal, with one peak near γ_s and the other less than γ_s. For large substrate strains, the onset of a square-to-hexagonal transition occurs with clusters having square symmetry nearly commensurate with the underlying substrate and clusters having hexagonal symmetry with γ_p near the equilibrium lattice constant 1.35 μm.

particles leave the substrate when the interaction level is too low. Calculations show gravitational effects are more than one order of magnitude smaller. We find the parameters $a = 65$ and $E_0/k_BT = 2.27$ reproduce the dependence of $\Delta F_{s/us}/k_BT$ on uniaxial strain as measured in the experiments (Fig. 3*B*). This free-energy dependence on strain is dramatically reduced when the range of the interaction is increased ($a = 6$; Fig. 3*B*), further illustrating the sensitivity of this phenomenon to the interaction range. Using the parameters that reproduce the uniaxial strain experiments, we performed simulations of single particle pairs on a crystalline layer of particles possessing square symmetry and isotropic strain. In agreement with our experimental results (Fig. 2), we find the particle strain γ_p is substantially lower than the substrate strain for intermediate γ_s (Fig. 4*A*).

We focus on the data for $\gamma_s = 0.03$, where $P(r)$ has a single peak l_p well beyond the interaction range (Fig. 4*B*). Because bond formation at this pair separation cannot be fully explained by the potential energy arising from the depletion interaction, it is important to quantify how both the bond energy and entropy affect particle positions. Fig. 4*C* shows the total potential energy U due to all interparticle bonds as a function of $(z - z_0)/l_0$ and r/l_0, where z is the average height of the particle pair, z_0 is the equilibrium height of a particle at an underlying lattice site, and r is the separation between particle pairs. These data show the radial position of the energetic minimum shifts to lower interparticle separations r/l_0 with increasing $(z - z_0)/l_0$. Using the probability distribution $P(r, z)$ in conjunction with our measurements for U, we determine the entropy ΔS increases rapidly with increasing $(z - z_0)/l_0$ (Fig. 4*D*) but hardly depends on r (Fig. S1).

The temperature-dependent probability p_{cryst} that neighboring crystallizing particles are bonded can be approximated by reflecting twice the probability distribution $P(r/l_0 < 1)$ about the line $r/l_0 = 1$, as shown by the blue shaded area in Fig. 4*B*. This region approximates $P(r)$ for an unstrained crystal, because it is symmetric, peaks at l_0, and, in the limit of zero strain, integrates to $p_{\text{cryst}} \sim 1$. Continuing to focus on data for $\gamma_s = 0.03$, we varied temperature to explore the role of entropy in particle bonding at fixed strain for various particle configurations (Fig. 4*E*). We find increasing temperature increases thermal fluctuations, increasing entropy by biasing $P(r, z)$ toward higher $(z - z_0)/l_0$ and decreasing r/l_0, resulting in smaller lattice constants than those imposed by the underlying substrate. Consequently, the combination of energy and entropy produces a substantial fraction of bonded particles, which leads to the observed crystals. At low temperatures—small thermal fluctuations—particles reside near substrate lattice sites. Because p_{cryst} is small, particles are not bound to one another, and crystals do not form. Remarkably, these results show lowering temperature causes crystals to dissolve. This mechanism of entropy-driven thermal fluctuations opposes the typical picture of freezing, whereby crystallization occurs upon lowering temperature. The traditional scenario is realized for the larger interaction range ($a = 6$), where lowering temperature increases the probability of bonding and hence crystallization. This difference further highlights the unique contributions of entropy due to thermal fluctuations in systems with very short-range interactions.

These results reveal a process in which entropy-driven thermal fluctuations stabilize crystal formation on substrates with lattice constants significantly larger than the interaction range. Although previous work has described particle crystallization on strained lattices under the influence of depletion potentials (23), the results presented here elucidate the role of entropy in increasing the interaction length of the depletion-induced bonding and the resulting reentrant phase transitions that arise. Our

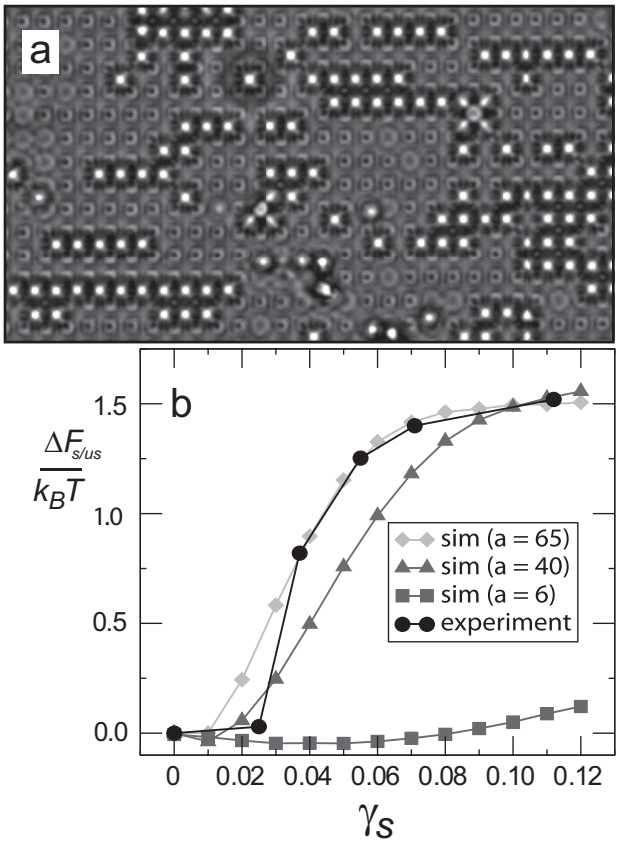

Fig. 3. Uniaxial strain to direct self-assembly. (*A*) Image of clusters formed on a uniaxially strained substrate with lattice constant 1.500 μm along the strained direction. Particle bonds preferentially form along the unstrained direction (horizontal), resulting in anisotropic, chain-like structures. (*B*) Experimental and simulated measurements of the free-energy cost for dimer formation along the strained direction relative to the unstrained direction. Dimers continue to form at substrate strains γ_s much larger than the interparticle interaction length scale ($\gamma_s \sim 0.02$). As the range of the potential is increased ($a = 6$), the free-energy cost of strain is dramatically reduced.

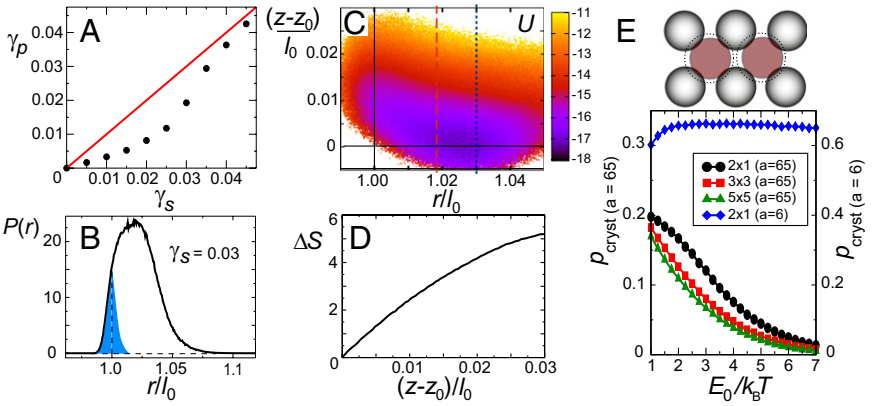

Fig. 4. Simulations on isotropically strained substrates. (*A*) Particle strain γ_p as a function of substrate strains γ_s for particle pairs. (*B*) $P(r)$ for $\gamma_s = 0.03$. The blue shaded region represents the contribution to $P(r)$ due only to the interaction potential. (*C*) Total potential energy U for particle pairs as a function of interparticle distance r/l_0 and height above the substrate $(z - z_0)/l_0$. As seen in experiments, the peak of $P(r)$ (red dashed line) is between the equilibrium lattice constant (black solid lines) and the substrate lattice constant (blue dotted line). (*D*) Entropic contribution ΔS to free energy as a function of average particle height above the substrate, $(z - z_0)/l_0$. (*E*) Probability of forming bonds as a function of decreasing temperature. For the short-range interaction ($a = 65$), crystals dissolve when the temperature is lowered, depicted in the cartoon as noninteracting particles constrained to lattice sites. For a longer-range system ($a = 6$), lowering temperature increases the probability of bond formation.

results and calculations have direct bearing on heterogeneous crystallization of globular proteins and nanoparticles (26). Specifically, they clarify how the free energy changes with temperature. As illustrated by Fig. 3, these results also suggest direct application in the burgeoning field of directed self-assembly, where modulating strain in the underlying substrate could be used to control crystal nucleation and growth. For example, we envision designer templates to assemble crystals having specific size and shape or plasmonic circuits whose configurations are tailored to produce desired electro-optical properties for applications in photonics, display technology, and electronics.

Methods

Sample Preparation. Samples are prepared by adding NaCl (4 mM) to deionized water, after which the nonionic surfactant $C_{12}E_6$ is added (2 wt%). Once the surfactant has equilibrated, polystyrene particles (3% polydispersity; Molecular Probes) are added to the solution. Templates are fabricated by spinning 500 nm poly(methyl methacrylate) onto a microscope coverslip and using electron beam lithography to pattern holes with a diameter of 1.26 μm. The sample is injected into a sample cell formed between the patterned coverslip and a microscope slide with a 170-μm spacer used to set the gap in height. The sample cell is sealed to prevent flow. Temperature control is accomplished by attaching an objective heater to a 100× (1.4 NA) objective and encasing the inverted microscope in a heated chamber with temperature fluctuations ±0.1 °C. All data are acquired after the temperature has equilibrated using bright-field microscopy.

Computer Simulations. Monte Carlo simulations using the standard Metropolis criterion were applied. To calculate the probability a dimer arranged parallel or perpendicular to the strained direction in the uniaxially strained case, the Monte Carlo moves also contain rotations of the dimer to generate the large number of transitions between orientations. Free-energy differences are calculated from the Boltzmann probability distribution. Using the Morse potential energy then gives the entropic contribution. We restrict the height of the second-layer particles to $(z - z_0)/l_0 \leq 0.03$ because for larger distances above the bottom layer, particles would start to desorb.

ACKNOWLEDGMENTS. The authors thank James Sethna for comments. This work is supported in part by Award KUS-C1-018-02 from King Abdullah University of Science and Technology, by a National Science Foundation Division of Materials Research Career award, and by the National Nanotechnology Infrastructure Network. S.F.H. and A.H. are grateful for the support by Transregio 61 and Sonderforschungsbereich 858 (DFG).

1. Turnbull D (1950) Kinetics of heterogeneous nucleation. *J Chem Phys* 18:198.
2. Auer S, Frenkel D (2003) Line tension controls wall-induced crystal nucleation in hard-sphere colloids. *Phys Rev Lett* 91(1):015703.
3. Sear R-P (2007) Nucleation: Theory and applications to protein solutions and colloidal suspensions. *J Phys Condens Matter* 19:033101.
4. Cacciuto A, Frenkel D (2005) Simulation of colloidal crystallization on finite structured templates. *Phys Rev E Stat Nonlin Soft Matter Phys* 72(4 Pt 1):041604.
5. Chayen N-E, Saridakis E, Sear R-P (2006) Experiment and theory for heterogeneous nucleation of protein crystals in a porous medium. *Proc Natl Acad Sci USA* 103(3):597–601.
6. Frenkel J-I, Kontorova T (1938) *Zh Eksp Teor Fiz* 8:1340–1348.
7. Brune H, et al. (1995) Effect of strain on surface diffusion and nucleation. *Phys Rev B Condens Matter* 52(20):14380–14383.
8. Zhang Z-Y, Lagally M-G (1997) Atomic processes in the early stages of thin-film growth. *Science* 276(5311):377–383.
9. Tersoff J, LeGoues FK (1994) Competing relaxation mechanisms in strained layers. *Phys Rev Lett* 72(22):3570–3573.
10. Barth J-V, Costantini G, Kern K (2005) Engineering atomic and molecular nanostructures at surfaces. *Nature* 437(7059):671–679.
11. Shevchenko EV, Talapin DV, Kotov NA, O'Brien S, Murray CB (2006) Structural diversity in binary nanoparticle superlattices. *Nature* 439(7072):55–59.
12. Gasser U (2009) Crystallization in three- and two-dimensional colloidal suspensions. *J Phys Condens Matter* 21(20):203101.
13. Galkin O, Vekilov P-G (2000) Control of protein crystal nucleation around the metastable liquid-liquid phase boundary. *Proc Natl Acad Sci USA* 97(12):6277–6281.
14. Anderson V-J, Lekkerkerker H-N-W (2002) Insights into phase transition kinetics from colloid science. *Nature* 416(6883):811–815.
15. Lomakin A, Asherie N, Benedek G-B (1999) Aeolotopic interactions of globular proteins. *Proc Natl Acad Sci USA* 96(17):9465–9468.
16. Talapin D-V, Lee J-S, Kovalenko M-V, Shevchenko E-V (2010) Prospects of colloidal nanocrystals for electronic and optoelectronic applications. *Chem Rev* 110(1):389–458.
17. Xia Y, Yin Y, Lu Y, McLellan J (2003) Template-assisted self-assembly of spherical colloids into complex and controllable structures. *Adv Funct Mater* 13:907–918.
18. Crocker J-C, Grier D-G (1996) Methods of digital video microscopy for colloidal studies. *J Colloid Interface Sci* 179:298–310.
19. Van Blaaderen A, Ruel R, Wiltzius P (1997) Template-directed colloidal crystallization. *Nature* 385:321–324.
20. Yethiraj A, van Blaaderen A (2003) A colloidal model system with an interaction tunable from hard sphere to soft and dipolar. *Nature* 421(6922):513–517.
21. Franzrahe K, Nielaba P (2007) Entropy versus energy: The phase behavior of a hard-disk mixture in a periodic external potential. *Phys Rev E Stat Nonlin Soft Matter Phys* 76(6 Pt 1):061503.
22. Ganapathy R, Buckley M-R, Gerbode S-J, Cohen I (2010) Direct measurements of island growth and step-edge barriers in colloidal epitaxy. *Science* 327(5964):445–448.
23. Lin Kh, et al. (2000) Entropically driven colloidal crystallization on patterned surfaces. *Phys Rev Lett* 85(8):1770–1773.
24. Savage J-R, Blair D-W, Levine A-J, Guyer RA, Dinsmore A-D (2006) Imaging the sublimation dynamics of colloidal crystallites. *Science* 314(5800):795–798.
25. Savage J-R, Dinsmore A-D (2009) Experimental evidence for two-step nucleation in colloidal crystallization. *Phys Rev Lett* 102(19):198302.
26. Kotov N-A (2010) Chemistry. Inorganic nanoparticles as protein mimics. *Science* 330(6001):188–189.